THE JOURNAL OF BIOLOGICAL CHEMISTRY VOL. 286, NO. 36, pp. 31789–31798, September 9, 2011

Two Structures of an *N*-Hydroxylating Flavoprotein Monooxygenase

ORNITHINE HYDROXYLASE FROM PSEUDOMONAS AERUGINOSA[*S]

Received for publication, May 31, 2011, and in revised form, July 2, 2011 Published, JBC Papers in Press, July 13, 2011, DOI 10.1074/jbc.M111.265876

Jose Olucha, Kathleen M. Meneely, Annemarie S. Chilton, and Audrey L. Lamb[1]

From the Department of Molecular Biosciences, University of Kansas, Lawrence, Kansas 66045

The ornithine hydroxylase from *Pseudomonas aeruginosa* (PvdA) catalyzes the FAD-dependent hydroxylation of the side chain amine of ornithine, which is subsequently formylated to generate the iron-chelating hydroxamates of the siderophore pyoverdin. PvdA belongs to the class B flavoprotein monooxygenases, which catalyze the oxidation of substrates using NADPH as the electron donor and molecular oxygen. Class B enzymes include the well studied flavin-containing monooxygenases and Baeyer-Villiger monooxygenases. The first two structures of a class B *N*-hydroxylating monooxygenase were determined with FAD in oxidized (1.9 Å resolution) and reduced (3.03 Å resolution) states. PvdA has the two expected Rossmann-like dinucleotide-binding domains for FAD and NADPH and also a substrate-binding domain, with the active site at the interface between the three domains. The structures have NADP(H) and (hydroxy)ornithine bound in a solvent-exposed active site, providing structural evidence for substrate and cosubstrate specificity and the inability of PvdA to bind FAD tightly. Structural and biochemical evidence indicates that $NADP^+$ remains bound throughout the oxidative half-reaction, which is proposed to shelter the flavin intermediates from solvent and thereby prevent uncoupling of NADPH oxidation from hydroxylated product formation.

The ornithine hydroxylase from *Pseudomonas aeruginosa* (PvdA) catalyzes the FAD-dependent hydroxylation of the ornithine side chain amine using NADPH as the electron donor and molecular oxygen (1). As a microbial *N*-hydroxylating monooxygenase, PvdA is considered to be a member of the class B flavoprotein monooxygenases, which share the following characteristics. 1) FAD is a stably bound cofactor; 2) NADPH, but not NADH, serves as the electron-donating cosubstrate and remains bound during the oxidative half-reaction; 3) they are composed of FAD and NADPH dinucleotide-binding domains; and 4) they are encoded by a single gene (2). PvdA meets these requirements with some caveats: PvdA does not stably bind FAD (1), and no previous work documents structure or confirms $NADP^+$ binding through the oxidative half-reaction.

The known class B flavoprotein monooxygenases are divided into three subclasses (2). Microbial *N*-hydroxylating monooxygenases catalyze the hydroxylation of primary amines and include PvdA (1, 3, 4), the ornithine hydroxylase from *Aspergillus fumigatus* (SidA) (5, 6), and the lysine hydroxylases (7, 8). A mechanism for PvdA (Fig. 1*a*) has been proposed previously (4). In short, NADPH reduces the oxidized flavin in the reductive half-reaction. In the oxidative half-reaction, ornithine binding accelerates the addition of oxygen to the flavin and makes a short-lived peroxyflavin intermediate (which is slow to form and long-lived in the absence of ornithine), followed by the hydroperoxyflavin intermediate. The hydroperoxyflavin donates the distal oxygen atom to the ornithine, forming hydroxyornithine and the hydroxyflavin intermediate. The hydroxyflavin intermediate dehydrates to regenerate the oxidized flavin. The oxidized nicotinamide cofactor dissociates with the product such that the cycle can continue. Class B Baeyer-Villiger monooxygenases include cyclohexanone monooxygenase (CHMO)[2] from *Acinetobacter* sp., which catalyzes the insertion of oxygen in the cyclohexanone ring to form a lactone via a Criegee intermediate (Fig. 1*b*) (9). For CHMO, the reactive flavin intermediate is the peroxyflavin, and no hydroperoxyflavin intermediate is formed in the product-forming cycle. The bacterial flavin monooxygenase from *Methylophaga aminisulfidivorans* belongs to the final subclass: the flavin-containing monooxygenases (FMOs). This subclass comprises both eukaryotic and prokaryotic monooxygenases that are able to catalyze hydroxylation of the reactive heteroatoms nitrogen, sulfur, phosphorus, selenium, and iodine (2, 10). Bacterial FMO (bFMO) catalyzes hydroxylation via the formation of a hydroperoxyflavin; however, no peroxyflavin intermediate is observed (Fig. 1*c*).

Here, we present two structures of the ornithine hydroxylase from *P. aeruginosa*, which are the first structures of a member of the microbial *N*-hydroxylating flavoprotein monooxygenase subclass. The enzyme structures are each mechanistically relevant ternary complexes, one in the oxidized state and one

* This work was supported, in whole or in part, by National Institutes of Health Graduate Training Program in Dynamic Aspects of Chemical Biology Grant T32 GM08545 from NIGMS (to J. O. and K. M. M.) and by National Institutes of Health Grant P20 RR016475 from the IDeA Networks of Biomedical Research Excellence Program of the National Center for Research Resources and Grant K02 AI093675 from NIAID (to A. L. L.).

[S] The on-line version of this article (available at http://www.jbc.org) contains supplemental Fig. S1.

The atomic coordinates and structure factors (codes 3S5W and 3S61) have been deposited in the Protein Data Bank, Research Collaboratory for Structural Bioinformatics, Rutgers University, New Brunswick, NJ (http://www.rcsb.org/).

[1] To whom correspondence should be addressed: Dept. of Molecular Biosciences, University of Kansas, 1200 Sunnyside Ave., Lawrence, KS 66045. Tel.: 785-864-5075; Fax: 785-864-5294; E-mail: lamb@ku.edu.

[2] The abbreviations used are: CHMO, cyclohexanone monooxygenase; FMO, flavin-containing monooxygenase; bFMO, bacterial FMO; SeMet, selenomethionine; r.m.s.d., root mean square deviation.

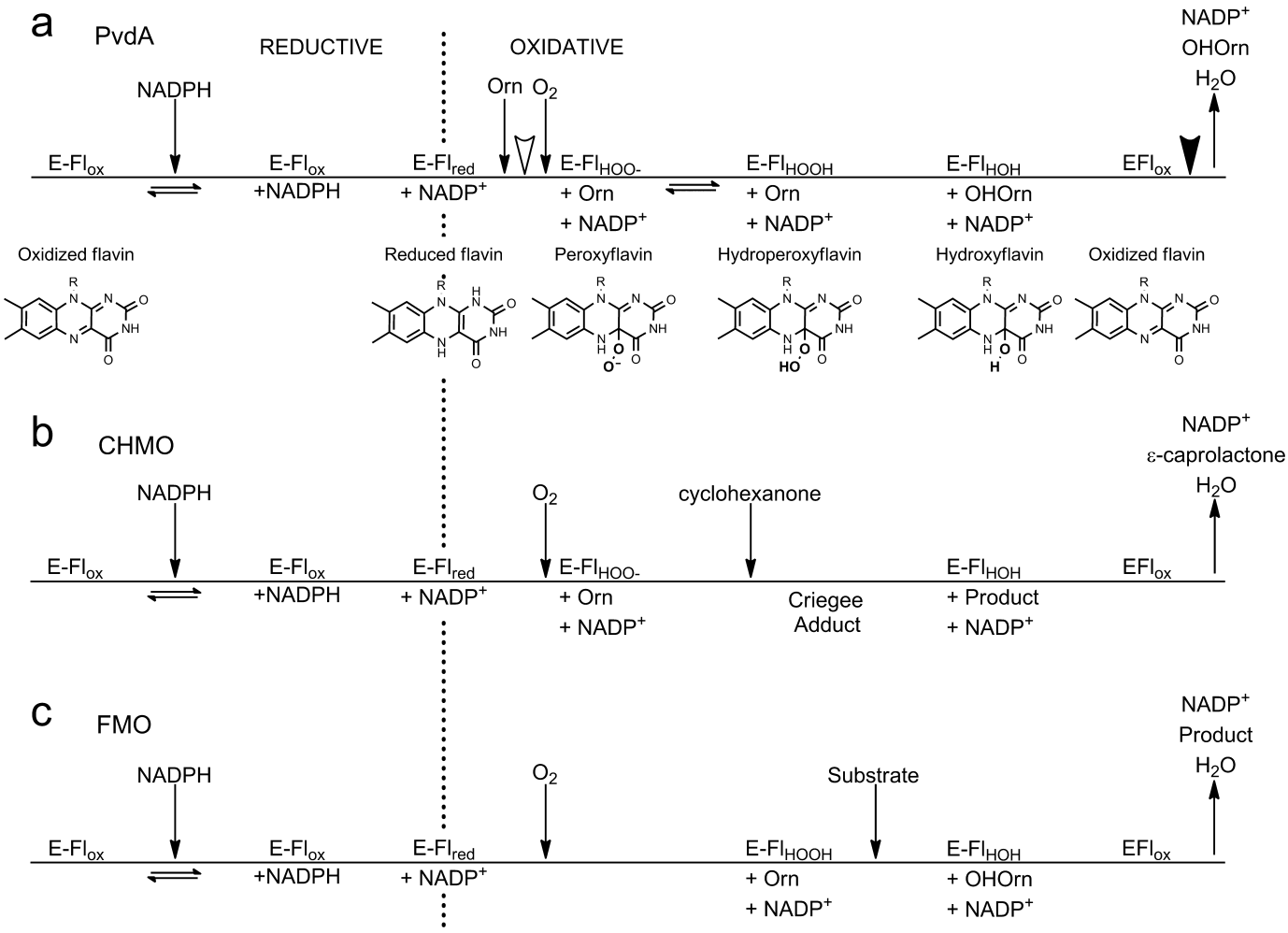

FIGURE 1. **Reactions catalyzed by ornithine hydroxylase (PvdA) (*a*), CHMO (*b*), and bFMO (*c*).** The flavin states are oxidized (Fl_{ox}), reduced (Fl_{red}), C4a-peroxyflavin intermediate (Fl_{HOO-}), hydroperoxyflavin intermediate (Fl_{HOOH}), and hydroxyflavin intermediate (Fl_{HOH}). For PvdA, the *open* and *closed arrowheads* represent the points in the catalytic cycle for the reduced and oxidized structures, respectively. *OHOrn*, hydroxyornithine.

in the reduced state. These structures are compared with those determined previously for CHMO from *Rhodococcus sp* HI-31 (11) and bFMO (12), highlighting the diversity of mechanisms for binding substrate within the members of the class B monooxygenases. We provide evidence that $NADP^+$ remains bound throughout the oxidative half-reaction for PvdA. Finally, we postulate that the two structures represent the reduced structure poised for oxygen binding and catalysis and the oxidized structure prior to product release.

EXPERIMENTAL PROCEDURES

Preparation of Oxidized PvdA and Selenomethionine (SeMet) PvdA—PvdA was cloned, overexpressed, and purified as described previously (1). The method for overexpression of SeMet PvdA was adapted from the protocol of Van Duyne *et al.* (13) with several modifications. M9 minimal medium was inoculated with 10 ml of overnight culture/liter of medium. The methionine biosynthesis pathway was inhibited by the addition of 100 mg each of L-lysine, L-phenylalanine, and L-threonine; 50 mg each of L-isoleucine, L-leucine, and L-valine; and 60 mg of DL-selenomethionine per liter of culture. Fifteen minutes after the addition of the amino acid mixture, protein expression was induced with the addition of isopropyl β-D-thiogalactopyranoside to a final concentration of 400 μM. SeMet PvdA was purified using the same protocol as that used for oxidized PvdA with the addition of 1 mM β-mercaptoethanol to all buffers.

Crystallization of Oxidized PvdA—Oxidized PvdA crystals were obtained through the hanging drop vapor diffusion method with a well solution containing 9.5% (w/v) PEG 8000, 25% (v/v) glycerol, and 60 mM monobasic potassium phosphate (pH 5.0). A solution of 16 mg/ml PvdA was incubated with FAD, NADPH, and L-ornithine to a final molar ratio of 1:3:20:150 (protein/FAD/NADPH/L-ornithine) on ice for 30 min. Three-microliter drops with a 1:1 ratio of protein to well solution were prepared over 600 μl of well solution. Rod-shaped yellow crystals grew to a size of 200 × 50 × 50 μm in 3 days at 18 °C.

Crystallization of SeMet PvdA—Crystals of SeMet PvdA were obtained under similar conditions to those described for oxidized PvdA (8% (w/v) PEG 8000, 15% (v/v) glycerol, and 80 mM MES (pH 5.5)). To keep a reduced environment, 10 μl of 1 M β-mercaptoethanol was added to each well. The protein solution was prepared with FAD, NADPH, and ornithine at the same ratios as used for oxidized PvdA. SeMet PvdA crystals

grew to a size of 150 × 40 × 40 μm in 5 days at 18 °C at a protein concentration of 9 mg/ml in 2-μl drops.

Production of Reduced PvdA Crystals—A flake of sodium dithionite was added to a drop containing oxidized PvdA crystals. The drop and crystals were monitored for a change from yellow to colorless for 30 min.

Preparation of Crystals for Data Collection—Oxidized PvdA crystals were harvested and transferred to a mother liquor drop with 11% (w/v) PEG 8000, 60 mM monobasic potassium phosphate, 20% (v/v) glycerol, 21 mM FAD, 41 mM NADPH, and 166 mM L-ornithine. SeMet PvdA crystals were harvested and transferred to a cryoprotectant with the same composition as used for the oxidized PvdA cryoprotectant with the addition of 2 mM β-mercaptoethanol. Reduced PvdA crystals were harvested and transferred to a cryoprotectant with the same composition as used for the oxidized PvdA cryoprotectant with the addition of sodium dithionite as described above. All crystals were flash-cooled to 77 K by plunging in liquid nitrogen.

Data Collection, Processing, and Structure Determination for SeMet PvdA—Multiwavelength anomalous dispersion experimental data for the SeMet PvdA crystal were collected at beamline 9-2 at the Stanford Synchrotron Radiation Lightsource. Peak (0.979112 Å), inflection (0.979304 Å), and remote (0.918402 Å) wavelengths were determined by a selenium fluorescence scan (K-edge, 12.6578 keV). Data (120°) were collected in 0.5° oscillation images with an exposure time of 5 s. The detector distance was set to 360.5 mm. Data were indexed and scaled to 2.8 Å resolution using the XDS program package (14). AutoSolve and AutoBuild from the PHENIX software suite (15) were used to determine the location of 12 selenium atoms (figure of merit = 0.42, overall score = 63) and initial phase estimates and to build the initial model. The initial model was built with 750 residues. Data processing and phasing statistics are provided in Table 1.

Data Collection, Processing, and Structure Determination for Oxidized PvdA—Oxidized PvdA oscillation images (0.5° images for a total of 360 images) were collected at beamline 9-2 at the Stanford Synchrotron Radiation Lightsource. Ten-second exposures at a wavelength of 1 Å and a detector distance of 200 mm were used. There was no evidence of radiolytic reduction of the oxidized crystals during the time course of the diffraction experiment. Data were scaled and indexed to 1.95 Å resolution using XDS (14). Because the SeMet and oxidized crystals were isomorphous, the initial SeMet model and phase estimate were used to build the higher resolution oxidized PvdA model using Refmac5 (16). Further model building and refinement of the structure were accomplished using Coot (17) and Refmac5 from the CCP4 software suite (16).

Data Collection, Processing, and Structure Determination for Reduced PvdA—Data for reduced PvdA were collected at beamline 9-2 at the Stanford Synchrotron Radiation Lightsource. Oscillation images (120° in 0.25° increments) were collected with 5-s exposures at a wavelength of 0.97946 Å and a detector distance of 408 mm. Data were scaled and indexed to 3.03 Å using XDS (14). Molecular replacement structure determination was performed with Phaser (18) from the CCP4 software suite using chain B of the oxidized structure with FAD, $NADP^+$, hydroxyornithine, and water omitted from the model. Further model building and refinement were accomplished using Coot (17) and Refmac5 (16).

Oxidized PvdA Crystallographic Model—The final oxidized PvdA model contains two monomers per asymmetric unit. The following residues are disordered in the structure: chain A, residues 1–9, 199–205, 360, and 428–443; and chain B, residues 1–9, 200–206, and 420–443. Both monomers have FAD, $NADP^+$, and hydroxyornithine in the active site. The $NADP^+$ nicotinamide moiety and ribose in the chain A active site are not modeled due to poor electron density, nor is the nicotinamide moiety in chain B. The model includes 376 waters and 4 phosphate molecules. Ramachandran analysis as calculated by PROCHECK (19) showed good geometry and angles, with 90.8% of the residues in allowed regions and 9.2% in additionally allowed regions.

Reduced PvdA Crystallographic Model—The reduced PvdA model contains two monomers per asymmetric unit. Both chains A and B have poor or no electron density for residues 1–8, 200–207, and 428–443. In addition, residues 359 and 360 are disordered in chain B. Both chains contain $FADH_2$, ornithine, and NADPH in the active site. In contrast to the oxidized model, the NADPH nicotinamide moiety is modeled in both active sites. Although density for ornithine was present in the reduced active site, it was not as well defined as the density of the hydroxyornithine in the oxidized structure.

Structural Analysis—All root mean square deviations were calculated using LSQMAN of the DEJAVU program suite (20). Protein structure figures were generated using PyMOL (21), and topology diagrams were generated using TopDraw (22).

Inhibition by $NADP^+$—The standard assay buffer contained 100 mM potassium phosphate (pH 8.0), 0.01 mM FAD, and 0–0.15 mM NADPH, with $NADP^+$ concentrations ranging from 0 to 2 mM. PvdA (1 μM) was incubated in 1 ml of assay buffer for 2 min at 25 °C before the reaction was initiated by the addition of 5 mM L-ornithine. The NADPH oxidation was monitored at 366 nm (ϵ = 2850 M^{-1} cm^{-1}) using a Cary 50 Bio spectrophotometer (Varian) and an electrothermal single cell holder for temperature control (±0.1 °C) at 25 °C for 120 s with 2-s time points according to the protocol described previously (1). All experiments were conducted in triplicate with standard deviations as indicated.

RESULTS

Overall Architecture—Initial phase estimates for PvdA were determined by multiwavelength anomalous dispersion phasing using a selenomethionine-substituted form of the protein (Table 1). The SeMet model was used as a starting point for structure refinement of the oxidized protein using a 1.9 Å isomorphous data set. The asymmetric unit contains two monomers of PvdA, related by a non-crystallographic 2-fold axis. The interface between the monomers buries ~950 $Å^2$ as calculated by PROTORP (23), which is in the range for homodimer formation (24); however, the biological assembly is assumed to be the monomer because dynamic light scattering observations provide a hydrodynamic radius indicative of a monomer in solution (1). Each monomer of PvdA comprises three well defined domains linked by flexible loops (Fig. 2). The FAD-

TABLE 1

Data collection and refinement statistics

All data were collected at beamline 9-2 at the Stanford Synchrotron Radiation Lightsource. Values in parentheses are for the highest resolution shells: 2.84 to 2.7 Å for SeMet data, 2.0 to 1.9 Å for oxidized data, and 3.19 to 3.03 Å for reduced data.

	SeMet				
	Peak	Inflection	Remote	Oxidized	Reduced
Data collection					
Wavelength (Å)	0.9791	0.9793	0.9184	1.000	0.9795
Space group		$I4_122$		$I4_122$	$I4_122$
Unit cell (Å)		$a = b = 130.94$, $c = 316.50$		$a = b = 130.94$, $c = 318.52$	$a = b = 128.16$, $c = 316.51$
Resolution range (Å)		36.6–2.7		36.8–1.9	39.26–3.03
Completeness (%)	99.7 (98.4)	99.7 (97.6)	99.7 (98.4)	99.5 (97.5)	99.4 (96.0)
Total reflections	275,715	275,906	275,985	741,798	246,515
Unique reflections	37,946	37,964	37,949	108,180	26,002
I/σ	17.1 (4.4)	17.1 (4.5)	19.0 (4.6)	15.3 (4.1)	25.1 (5.8)
R_{sym} (%)[a]	9.1 (42.1)	9.1 (42.8)	8.8 (42.9)	6.7 (41.2)	8.0 (40.7)
Multiplicity	7.3 (7.3)	7.3 (7.3)	7.3 (7.3)	6.9 (6.5)	9.5 (9.2)
No. of refined selenium sites		12			
Anomalous correlation between half-sets[b]	0.36	0.33	0.16		
Mean figure of merit[c]		0.42		0.97	0.91
Mid-slope of anomalous probability[d]	1.2	1.2	1.1		
Refinement					
Resolution range (Å)				36.74–1.90	39.26–3.03
No. of reflections				102,726	23,360
R-factor[e]				19.2	21.5
R_{free}				21.7	27.1
No. of protein/non-hydrogen atoms				6561	6541
No. of ligand and solvent atoms				584	220
Ramachandran allowed (%)				100	100
r.m.s.d. bond length (Å)				0.0154	0.0162
r.m.s.d. bond angle				1.56°	1.89°
Average B (Å^2)					
Protein				32.0	59.0
Ligands				27.4	68.0
Water				33.5	Not applicable

[a] $R_{sym} = \Sigma|I - \langle I\rangle|/\Sigma|$, where I is the observed intensity and $\langle I\rangle$ is the statistically weighted absolute intensity of multiple measurements of symmetry-related reflections.
[b] Anomalous correlation between half-sets = $\Sigma\|FPH \pm FP| - FH_{calc}|/\Sigma|FPH|$ reported for all centric reflections.
[c] Mean figure of merit = $\langle\alpha\Sigma P_\alpha e^{i\alpha}/\Sigma P_\alpha\rangle$, where a is the phase and P_α is the phase probability distribution.
[d] Mid-slope of anomalous probability = $\langle|FH|/\|FP + FH| - |FPH\|\rangle$ reported for all reflections.
[e] $R = \Sigma|F_o - |F_c\||/\Sigma|F_o|$ (R from the working set and R_{free} from the test set). Ten percent of the reflections were reserved for the calculation of R_{free}.

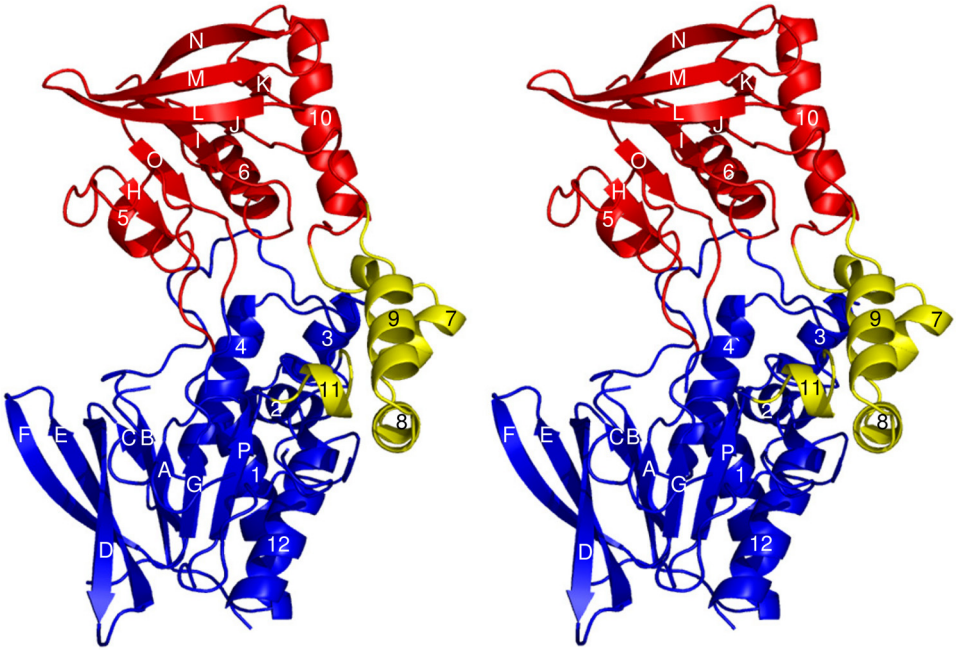

FIGURE 2. **Stereoview of the overall architecture of PvdA.** The FAD-binding domain is shown in *blue*, the NADPH-binding domain in *red*, and the ornithine-binding domain in *yellow*. Strands are denoted by letters *A–P*, starting from the N terminus. Helices are counted from the N terminus, *1–12*.

binding domain is the largest of the three domains (250 residues) and is folded into an α/β-nucleotide-binding architecture. This domain is composed of residues from three separate segments belonging to the N and C termini: residues 1–171, 356–396, and 405–443. The NADPH-binding domain is composed of 144 residues, and also folds into an α/β-nucleotide-binding fold. This domain includes residues 170–245 and 285–355. The smallest domain is the ornithine-binding domain,

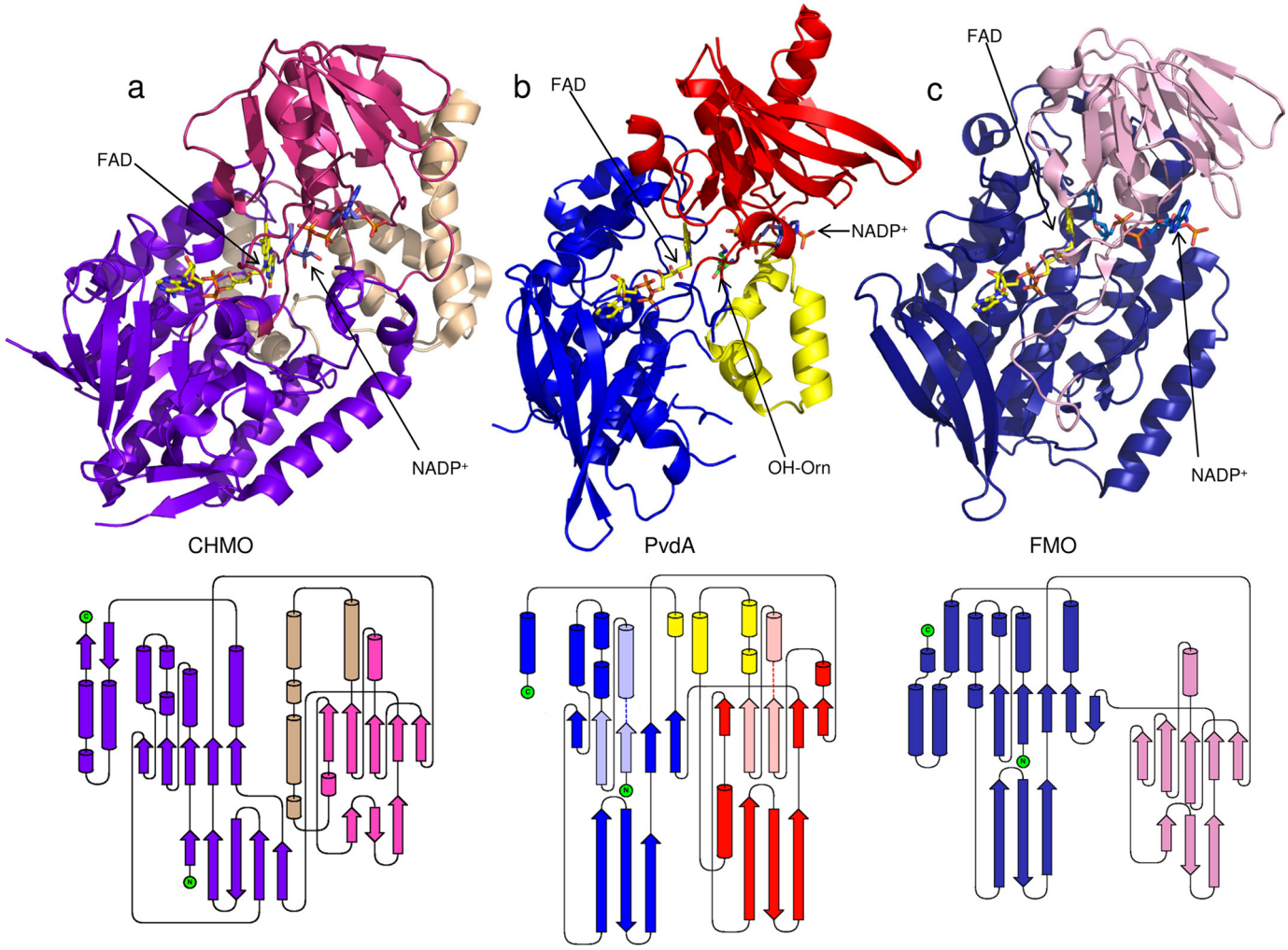

FIGURE 3. **Schematics and topology diagrams of CHMO (Protein Data Bank code 3GWD) (*a*), PvdA (*b*), and bFMO (code 2VQ7) (*c*).** The FAD-binding domains are shown in *blue/purple*, the NADPH-binding domains in *red/pink*, and the substrate-binding domains in *yellow/tan*. In the schematics, the proteins are aligned by the orientation of FAD, shown as *yellow sticks*. NADPH is shown as *blue sticks*, and the product (PvdA only, hydroxyornithine) as *green sticks*. In the PvdA topology diagram, the $\beta\alpha\beta$-motif for dinucleotide binding is shown in a lighter shade (*light blue*, FAD; *pink*, NADPH), and the loop containing the consensus sequence is a similarly colored *dashed line*.

comprising 45 residues (248–285 and 398–404) that form four small helices.

PvdA Is Structurally Distinct from Other Class B Monooxygenases—A protein structural comparison using the service Fold at the European Bioinformatics Institute (25) suggested that PvdA shared approximately similar structural homology with a wide range of flavin-dependent enzymes, with none significantly more similar than the class B monooxygenases. Least-squares superpositioning of bFMO (the most similar from this subclass) and PvdA using LSQMAN (20) indicated a root mean square deviation (r.m.s.d.) of 1.8 Å over 213 aligned Cα atoms of the possible 414 modeled α-carbons in the PvdA structure, with the predominance of the structural similarity in the FAD-binding domain (r.m.s.d. of 1.6 Å for 163 Cα atoms) and some similarity in the NADPH-binding domain (r.m.s.d. of 2.0 Å for 58 Cα atoms). A structural alignment between closed CHMO (the most similar from the Baeyer-Villiger monooxygenase subclass) and PvdA provided a r.m.s.d. of 1.8 Å over 263 Cα atoms aligned. The structural similarity was highest in the FAD-binding domain (r.m.s.d. of 1.7 Å for 157 Cα atoms) and NADPH-binding domain (r.m.s.d. of 2.0 Å for 93 Cα atoms), with some structural similarity in the substrate-binding domains (r.m.s.d. of 2.2 Å for 13 Cα atoms). A side-by-side comparison of PvdA with FMO and CHMO, as well as a topology comparison, is shown in Fig. 3. It is immediately evident that PvdA is a smaller protein. Whereas the topologies of the individual FAD- and NADPH-binding domains share similarities expected for Rossmann-like domains, they are distinct among the three proteins. Furthermore, FMO does not possess a substrate-binding domain, as found in both PvdA and CHMO.

FAD-binding Domain—The FAD molecule is in an elongated conformation with the isoalloxazine-flavin ring structure at the interface of all three domains. The architecture of the FAD-binding domain is an α/β-fold characteristic of the glutathione reductase structural family of flavoproteins (26). In PvdA, this domain comprises two β-sheets and five helices. The central sheet contains five parallel strands that are flanked on one side by a three-stranded antiparallel sheet and on the other by the helices (Fig. 3). The nucleotide-binding consensus sequence

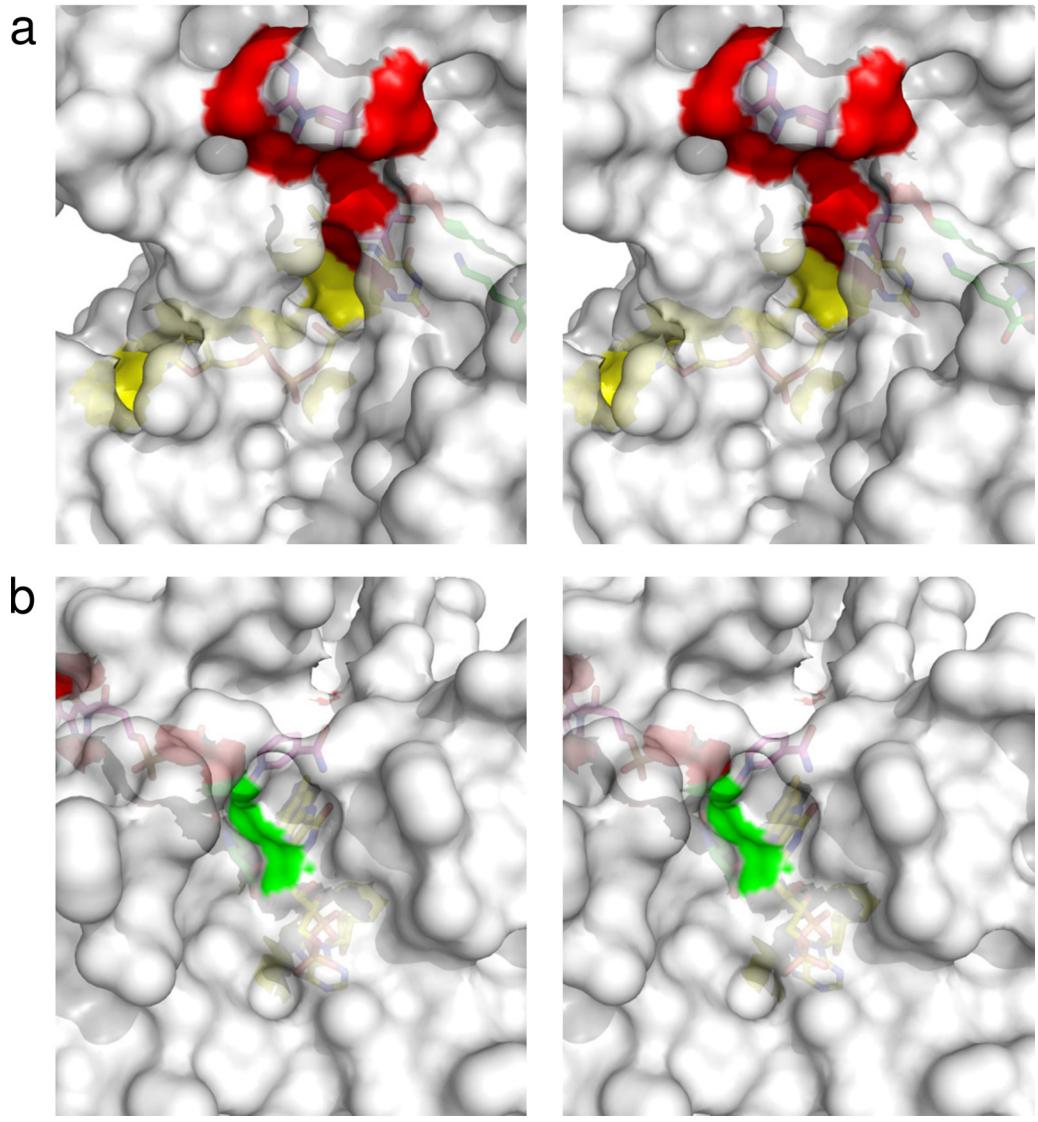

FIGURE 4. **Stereo diagrams of the solvent-accessible surface of the reduced PvdA structure, highlighting that the ligands make up significant portions of the "surface" of this structure.** Protein surface is *white* and partially transparent, FAD is *yellow*, NADPH is *red*, and ornithine is *green*. The ligands are shown as *sticks*, but the amino acids are not. *a* and *b* are related by a 120° rotation about the *y axis*.

(G*X*G*XX*G) is located in a conserved dinucleotide-binding $\beta\alpha\beta$-motif, which in flavin-binding domains forms a dipole-charge interaction between the N terminus of the helix and the diphosphate moiety of FAD. However, the loop between strand A and helix 1 in PvdA is not the characteristic tight turn (**G*X*G***XX*G**) but has three amino acids (**G*XG***XX*G**). Furthermore, the sequence is not completely conserved in PvdA, with the final residue being an asparagine (G*X*G*XX*N). This asparagine (Asn-22 of helix 1) forms a hydrogen bond from the side chain nitrogen to the backbone carbonyl of Gly-17 (the first glycine of the consensus sequence). The side chain oxygen of Asn-22 forms a hydrogen bond with the side chain nitrogen of Gln-395 of strand P. This hydrogen bond network may serve to stabilize the longer loop between strand A and helix 1. Finally, unlike the other class B monooxygenases, the FAD cofactor is not as buried in the dinucleotide-binding cleft (Fig. 4) but is solvent-exposed, most probably explaining why PvdA does not bind FAD tightly.

NADPH-binding Domain—The NADPH molecule is also bound in an elongated conformation at an analogous position to that of FAD in the α/β-nucleotide-binding architecture of the NADPH-binding domain. As with the FAD-binding domain, the NADPH-binding domain contains a central sheet of five parallel strands that are flanked on one side by a three-stranded antiparallel sheet and on the other by helices (Fig. 3). A five-residue turn (residues 214–218) that connects strand I with helix 6 forms the analogous interaction loop for nucleotide binding. There is not sufficient electron density to model nicotinamide in the A or B chain or the nicotinamide ribose in the A chain. This flexibility in binding of the co-substrate is suggestive of motion in the active site that is required for catalysis. Two interactions provide structural evidence for the specificity of NADPH over NADH for PvdA (1). Arg-240 forms two hydrogen bonds with the phosphate of the adenine ribose, and the guanidinium forms a stacking interaction with the adenine moiety of the NADPH. An equivalent interaction is present in

CHMO (Arg-210) and bFMO (Arg-234), which are both NADPH-specific. Ser-286 also hydrogen bonds with this phosphate, equivalent to Ser-210 in bFMO. The equivalent interaction in CHMO is hypothesized to be Lys-329, for which there is biochemical evidence for cofactor specificity (27); however, although this lysine is proximal to the phosphate group, there are no direct interactions in either the open or closed CHMO structures (11).

Ornithine-binding Domain—The ornithine-binding domain is smallest of the three domains, composed of four helices forming a bundle. The helices are derived from the loop connecting strand P and helix 12 of the FAD-binding domain (helix 11) and from the loop connecting strand J and helix 10 of the NADPH-binding domain (helices 7–9). Whereas PvdA was incubated with FAD, NADPH, and ornithine prior to crystallization, there is clear density for the hydroxylated product, and this molecule has thus been modeled as hydroxyornithine. The hydroxyornithine lies in the cleft at the interface between the FAD- and ornithine-binding domain (Fig. 5, *a* and *c*). A network of hydrogen bonds and salt links includes five residues, two from the FAD-binding domain (Gln-64 and Lys-69) and three from the ornithine-binding domain (Asn-254, Thr-283, and Asn-284), that with two waters stabilize hydroxyornithine in the active site 5.5 Å away from the C4a atom of the isoalloxazine ring of FAD (Fig. 5*c*). Three of the stabilizing residues, Gln-64, Lys-69, and Asn-254, are located in flexible loops, whereas Asn-254 is located in helix 7 and Thr-283 in helix 9. Gln-64 forms a hydrogen bond with the newly formed hydroxyl group on the hydroxyornithine side chain. Asn-254 forms hydrogen bonds with both the carboxylate and amine of the ornithine main chain, and Lys-69 forms a salt bridge with the carboxylate, providing a clear basis for the exclusive L-amino acid specificity observed for this enzyme (1).

Reduced PvdA Structure—There are no large structural differences between the oxidized and reduced structures of PvdA. Indeed, superimposing the two structures in LSQMAN results in a r.m.s.d. of 0.4 Å for all Cα atoms (supplemental Fig. S1). The most significant differences between the two models lie in the active site itself (Fig. 5, *b* and *d*). Whereas there is no electron density for the nicotinamide moiety in the oxidized PvdA structure, the nicotinamide moiety has well defined electron density (for an ~3 Å structure) in both monomers of the reduced structure. The second significant difference between the two active sites is the poor electron density of the substrate in the reduced structure compared with the very well defined electron density of the product in the oxidized model. (There is no electron density for the hydroxyl group of the product, and this molecule is thus modeled as the ornithine substrate in the reduced structure.) This would suggest lower occupancy for ornithine binding in the active site when FAD is reduced. Two amino acid side chains have altered their conformations between the oxidized and reduced structures. Gln-64 is slightly rotated away from the ordered nicotinamide ring and has no hydrogen-bonding partner with the substrate (as opposed to the product). Asn-284 has rotated but remains hydrogen-bonded with the N^5-amine of the ornithine side chain. Finally, the reduced structure was determined to 3.03 Å, and thus, no ordered water molecules are observed in the active site.

$NADP^+$ Is a Competitive Inhibitor of NADPH—Inhibition assays indicated that $NADP^+$ is a competitive inhibitor of NADPH using the NADPH oxidation assay (Fig. 6), providing evidence that $NADP^+$ remains bound during the oxidative half-reaction. These data are consistent with those for the ornithine hydroxylase of *A. fumigatus*, for which it was argued that NADPH is the first substrate to bind and $NADP^+$ is the last product to dissociate (6).

DISCUSSION

This work provides the first structure of the *N*-hydroxylating monooxygenase subclass of the class B flavoprotein monooxygenases and allows for comparisons with enzymes from the other two subclasses. The global architecture is mostly consistent between the three subclasses, with two Rossmann-like dinucleotide-binding domains, one each for FAD and NADPH binding. The NADPH-binding domain is inserted into the FAD-binding domain, and an active site crevice is formed between the two. Even a cursory glance at Fig. 3 shows that the topology and domain arrangement between the three subclasses are distinct. The most obvious consideration is the substrate-binding domain. bFMO does not have a clearly delineated substrate cavity, whereas CHMO has a pocket derived from an apparent segment insertion of five helices in the NADPH-binding domain. The substrate-binding domain of PvdA is derived from two inserts, one from the FAD-binding domain and one from the NADPH-binding domain.

PvdA shows a clear biochemical preference for NADPH, with no activity with NADH (1). Arg-240 and Ser-286 provide interactions with the adenine phosphate, in keeping with this observation. Fig. 5 illustrates the multiple interactions with the ornithine substrate and hydroxyornithine product. The hydrogen-bonding pattern corroborates the biochemical evidence for substrate specificity (1): amino acids of shorter length do not serve as substrates, and the α-amine and carboxylate of ornithine can acquire ligand-binding interactions for only the L-form of the amino acid. Lysine (one methylene group longer) allows for NADPH oxidation, but no hydroxylated product is formed. In light of this model, it would be assumed that lysine binds similarly to ornithine using the same interactions at the main chain carboxylate and amine. As a consequence, this binding may cause the side chain amine to advance too far into the active site, no longer in a favorable position for hydroxylation. Furthermore, this binding would most likely promote the premature release of $NADP^+$ and cause the observed uncoupling with this substrate (1).

Importantly, this work provides the first structures of a class B enzyme in which three of the ligands (FAD, NADPH, and substrate/product) are bound simultaneously. Because FAD does not bind stably to PvdA in solution, it was highly fortuitous to observe FAD-bound PvdA crystals. Moreover, occupancy of the FAD-binding cleft no doubt facilitates the correct binding of both NADP(H) and (hydroxy)ornithine. The reduced structure has $FADH_2$ and NADPH (which are presumed to be reduced as a consequence of the observed bleaching of the distinct yellow color of the crystals when sodium dithionite is present in the soaking and cryoprotection solutions) and ornithine at low occupancy. The oxidized structure has oxidized FAD,

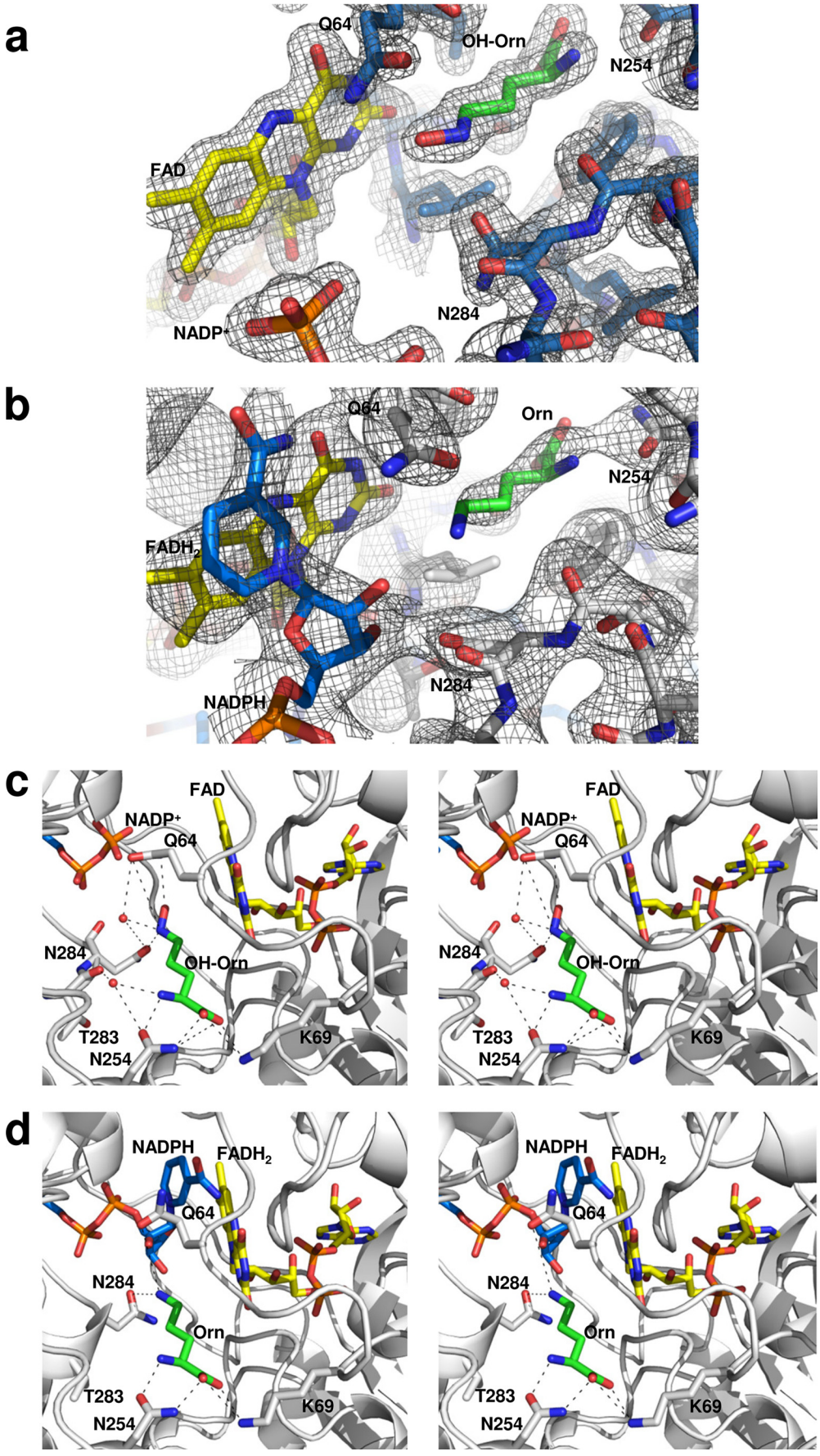
a
Q64
OH-Orn
N254
FAD
N284
NADP+
b
Q64
Orn
N254
FADH2
N284
NADPH
c
FAD
NADP+
Q64
N284
OH-Orn
T283
N254
K69
FAD
NADP+
Q64
N284
OH-Orn
T283
N254
K69
d
NADPH
FADH2
Q64
N284
Orn
T283
N254
K69
NADPH
FADH2
Q64
N284
Orn
T283
N254
K69

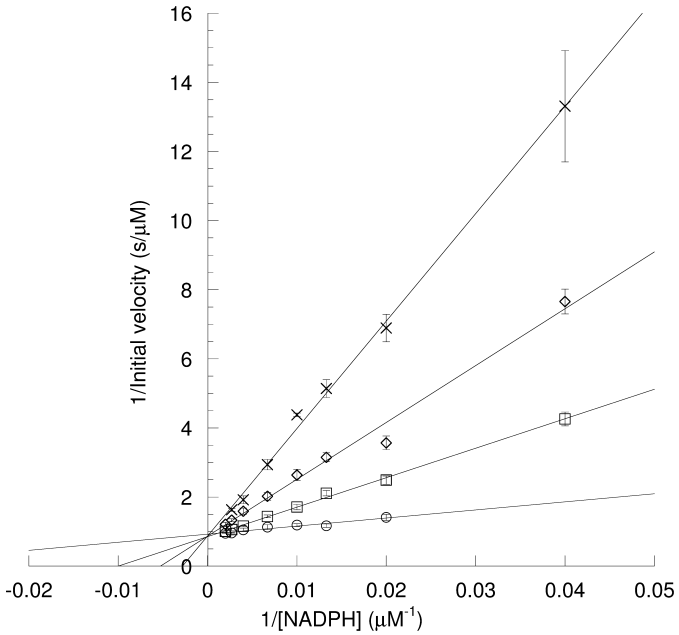

FIGURE 6. **$NADP^+$ is a competitive inhibitor of NADPH.** Shown is a double-reciprocal plot of NADPH oxidation as a function of NADPH concentration. $NADP^+$ was used at concentrations of 0 μM (○), 500 μM (□), 1000 μM (◇), and 2000 μM (×).

$NADP^+$, and the hydroxyornithine product. Previous structures of the class B enzymes all contain FAD, but none have both NADP(H) and substrate. Several structures of yeast and bacterial FMOs have been reported with NADP(H) or substrate but not both (12, 28–30). Two structures have been reported for CHMO (two conformations with $NADP^+$ bound) (11), as well as a structure for phenylacetone monooxygenase from *Thermobifida fusca* (a Baeyer-Villiger monooxygenase) with only FAD bound (31).

$NADP^+$ has been shown to stabilize the oxygen intermediates of the mammalian FMOs (32, 33), SidA (6), and CHMO (9). A hypothesis for how this is accomplished was presented with the structure of bFMO (12). A model of the C4a-hydroperoxyflavin was generated in which the oxygen of the flavin intermediate is within hydrogen-bonding distance of the ribose 2′-hydroxyl of the nicotinamide ribose of $NADP^+$, an $NADP^+$-binding mode that is shared by the reduced structure of PvdA. Recent structures of the same enzyme from a different group led to a counterproposal that the enzyme actually uses a ping-pong mechanism because the $NADP^+$-binding site overlaps with the determined substrate (indole)-binding side (28). Both groups cite the importance of a tyrosine residue (the same residue, Tyr-207 or Tyr-212, depending on the numbering by the authors) for organization of the nicotinamide in the active site. It should be noted that the bFMO structure with indole bound could be determined only in an active site variant enzyme in which this tyrosine was changed to serine. The variant form was inactive and showed a significant conformational change in the loop containing this residue after mutation. Arg-337 in phenylacetone monooxygenase (31) is located in a similar position to Tyr-207/212 in bFMO and has been hypothesized to be important in organizing the nicotinamide ring in the active site and hydrogen bonding to the hydroperoxyflavin intermediate. There is no comparable bulky or charged residue in the active site of PvdA or CHMO.

The PvdA active site is the most solvent-exposed of the known class B enzyme structures. Indeed, the active site is closed only by the binding of FAD, $NADP^+$, and ornithine (Fig. 4). Protection of the flavin intermediates from water is required for catalysis, and we therefore propose that a general role of $NADP^+$ in the oxidative half-reaction is to shelter the active site from solvent, thereby preventing uncoupling of the reaction in the form of hydrogen peroxide elimination rather than hydroxylation of ornithine. The open active site of PvdA explains the biochemical observations that FAD is not bound stably and that NADPH oxidation is very readily uncoupled from production of hydroxylated product (1, 4). The open active site also leads us to question one of our previous observations (4). Without a conformational change to close the cleft that binds ornithine, it seems unlikely that a long-lived peroxyflavin intermediate is possible in the absence of ornithine. There is crystallographic support for this idea: no crystals formed in the absence of ornithine, suggesting that there is a different conformational state without ornithine.

Asn-78 of bFMO has been suggested to be important in stabilizing flavin oxygen intermediates, with several mutants crystallized and tested kinetically (30). The N78D variant is the most interesting, as this change converts the enzyme from a monooxygenase to an oxidase. In PvdA, this amino acid is a glutamine (Gln-64); however, in CHMO and phenylacetone monooxygenase, this residue is an aspartic acid (Asp-59 and Asp-66, respectively). The hypothesis that an uncharged amino acid at this site is required for flavin intermediate stabilization may not be broadly applicable to all class B enzymes. Alternately, the aspartic acid in CHMO and phenylacetone monooxygenase could represent an adaptation necessary to carry out the Baeyer-Villiger reaction, in which the peroxyflavin intermediate is reactive with substrate and not the hydroperoxyflavin intermediate, as is the case for FMOs and *N*-hydroxylating monooxygenases.

CONCLUSIONS

$NADP^+$ remains bound to PvdA through the oxidative half-reaction. In the reduced structure, the nicotinamide ring is in a conformation that would indicate that reduction of the flavin has occurred and the ring has retracted to allow for oxygen binding. In the oxidized structure, the nicotinamide (and even one of the nicotinamide riboses of the two monomers) does not have electron density, indicating conformational flexibility. Nicotinamide mobility may allow for several binding modes

FIGURE 5. **Comparison of the oxidized and reduced active sites of PvdA.** *a* and *b*, electron density maps (*gray cages*) of the active sites are $2F_c - F_c$ maps contoured at 1.5σ for the oxidized and reduced structures, respectively. Oxygen atoms are *red*, nitrogen atoms are *dark blue*, and phosphorus atoms are *orange*. Carbons are colored as per the molecule: PvdA, *slate blue* or *gray*; $FAD(H_2)$, *yellow*; ornithine, *green*; and NADP(H), *bright blue*. There is no density for the nicotinamide moiety of $NADP^+$ in the oxidized form of the enzyme. *c* and *d*, stereo views of the active site of the oxidized and reduced structures respectively, using the same color scheme. Hydrogen bonds are shown as *dashed lines*.

throughout the catalytic cycle. This may be somewhat analogous to the mobile flavin of the class A enzymes (enzymes with a single dinucleotide-binding domain that release $NAD(P)^+$ immediately after flavin reduction), in which the flavin has been observed in "in" and "out" positions and is therefore hypothesized to move during catalysis (34–36). We propose that $NADP^+$ must remain bound throughout the catalytic cycle to form a closed active site suitable for formation of the flavin intermediates.

Acknowledgments—We are grateful to Dr. G. R. Moran for insightful discussions and critically reading this manuscript. Diffraction data were collected at the Stanford Synchrotron Radiation Lightsource, a national user facility operated by Stanford University on behalf of the Office of Basic Energy Sciences, United States Department of Energy. The Stanford Synchrotron Radiation Lightsource Structural Molecular Biology Program is supported by the Office of Biological and Environmental Research, United States Department of Energy; by the National Center for Research Resources Biomedical Technology Program, National Institutes of Health; and by NIGMS. We thank the staff at the Stanford Synchrotron Radiation Lightsource for support and assistance.

REFERENCES

1. Meneely, K. M., and Lamb, A. L. (2007) *Biochemistry* **46,** 11930–11937
2. van Berkel, W. J.., Kamerbeek, N. M., and Fraaije, M. W. (2006) *J. Biotechnol.* **124,** 670–689
3. Ge, L., and Seah, S. Y. (2006) *J. Bacteriol.* **188,** 7205–7210
4. Meneely, K. M., Barr, E. W., Bollinger, J. M., Jr., and Lamb, A. L. (2009) *Biochemistry* **48,** 4371–4376
5. Chocklett, S. W., and Sobrado, P. (2010) *Biochemistry* **49,** 6777–6783
6. Mayfield, J. A., Frederick, R. E., Streit, B. R., Wencewicz, T. A., Ballou, D. P., and DuBois, J. L. (2010) *J. Biol. Chem.* **285,** 30375–30388
7. Thariath, A., Socha, D., Valvano, M. A., and Viswanatha, T. (1993) *J. Bacteriol.* **175,** 589–596
8. Thariath, A. M., Fatum, K. L., Valvano, M. A., and Viswanatha, T. (1993) *Biochim. Biophys. Acta* **1203,** 27–35
9. Sheng, D., Ballou, D. P., and Massey, V. (2001) *Biochemistry* **40,** 11156–11167
10. Krueger, S. K., and Williams, D. E. (2005) *Pharmacol. Ther.* **106,** 357–387
11. Mirza, I. A., Yachnin, B. J., Wang, S., Grosse, S., Bergeron, H., Imura, A., Iwaki, H., Hasegawa, Y., Lau, P. C., and Berghuis, A. M. (2009) *J. Am. Chem. Soc.* **131,** 8848–8854
12. Alfieri, A., Malito, E., Orru, R., Fraaije, M. W., and Mattevi, A. (2008) *Proc. Natl. Acad. Sci. U.S.A.* **105,** 6572–6577
13. Van Duyne, G. D., Standaert, R. F., Karplus, P. A., Schreiber, S. L., and Clardy, J. (1993) *J. Mol. Biol.* **229,** 105–124
14. Kabsch, W. (2010) *Acta Crystallogr. D* **66,** 125–132
15. Adams, P. D., Afonine, P. V., Bunkóczi, G., Chen, V. B., Davis, I. W., Echols, N., Headd, J. J., Hung, L. W., Kapral, G. J., Grosse-Kunstleve, R. W., McCoy, A. J., Moriarty, N. W., Oeffner, R., Read, R. J., Richardson, D. C., Richardson, J. S., Terwilliger, T. C., and Zwart, P. H. (2010) *Acta Crystallogr. D* **66,** 213–221
16. Murshudov, G. N., Vagin, A. A., and Dodson, E. J. (1997) *Acta Crystallogr. D* **53,** 240–255
17. Emsley, P., and Cowtan, K. (2004) *Acta Crystallogr. D* **60,** 2126–2132
18. McCoy, A. J., Grosse-Kunstleve, R. W., Storoni, L. C., and Read, R. J. (2005) *Acta Crystallogr. D* **61,** 458–464
19. Laskowski, R., MacArthur, M., Moss, D., and Thornton, J. (1993) *J. Appl. Crystallogr.* **26,** 283–291
20. Kleywegt, G. J., and Jones, T. A. (1997) *Methods Enzymol.* **277,** 525–545
21. DeLano, W. L. (2002) *The PyMOL Molecular Graphics System*, DeLano Scientific LLC, San Carlos, CA
22. Bond, C. S. (2003) *Bioinformatics* **19,** 311–312
23. Reynolds, C., Damerell, D., and Jones, S. (2009) *Bioinformatics* **25,** 413–414
24. Jones, S., and Thornton, J. M. (1996) *Proc. Natl. Acad. Sci. U.S.A.* **93,** 13–20
25. Krissinel, E., and Henrick, K. (2004) *Acta Crystallogr. D* **60,** 2256–2268
26. Dym, O., and Eisenberg, D. (2001) *Protein Sci.* **10,** 1712–1728
27. Kamerbeek, N. M., Fraaije, M. W., and Janssen, D. B. (2004) *FEBS Lett.* **271,** 2107–2116
28. Cho, H. J., Cho, H. Y., Kim, K. J., Kim, M. H., Kim, S. W., and Kang, B. S. (2011) *J. Struct. Biol.* **175,** 39–48
29. Eswaramoorthy, S., Bonanno, J. B., Burley, S. K., and Swaminathan, S. (2006) *Proc. Natl. Acad. Sci. U.S.A.* **103,** 9832–9837
30. Orru, R., Pazmiño, D. E., Fraaije, M. W., and Mattevi, A. (2010) *J. Biol. Chem.* **285,** 35021–35028
31. Malito, E., Alfieri, A., Fraaije, M. W., and Mattevi, A. (2004) *Proc. Natl. Acad. Sci. U.S.A.* **101,** 13157–13162
32. Beaty, N. B., and Ballou, D. P. (1980) *J. Biol. Chem.* **255,** 3817–3819
33. Beaty, N. B., and Ballou, D. P. (1981) *J. Biol. Chem.* **256,** 4619–4625
34. Gatti, D. L., Palfey, B. A., Lah, M. S., Entsch, B., Massey, V., Ballou, D. P., and Ludwig, M. L. (1994) *Science* **266,** 110–114
35. Moran, G. R., Entsch, B., Palfey, B. A., and Ballou, D. P. (1996) *Biochemistry* **35,** 9278–9285
36. Palfey, B. A., Moran, G. R., Entsch, B., Ballou, D. P., and Massey, V. (1999) *Biochemistry* **38,** 1153–1158